

## Visualization of Phospholipid Particle Fusion Induced by Duramycin

Soichiro Matsunaga,<sup>†,‡</sup> Takuro Matsunaga,<sup>†,§</sup> Kunihiko Iwamoto,<sup>‡</sup> Taro Yamada,<sup>‡</sup>  
Mitsuhiro Shibayama,<sup>†,§</sup> Maki Kawai,<sup>\*,†,‡</sup> and Toshihide Kobayashi<sup>‡</sup>

<sup>†</sup>Department of Advanced Materials Science, The University of Tokyo, 5-1-5 Kashiwanoha, Kashiwa-shi, 277-8561, Japan, <sup>‡</sup>RIKEN (The Institute of Physical and Chemical Research), 2-1 Hirosawa, Wako-shi, 351-0198, Japan, and <sup>§</sup>Institute for Solid State Physics, The University of Tokyo, 5-1-5 Kashiwanoha, Kashiwa-shi, 277-8581, Japan

Received February 19, 2009. Revised Manuscript Received April 9, 2009

We visualized nanometer-scale phospholipid particle fusion by scanning tunneling microscopy (STM) on an alkanethiol-modified gold substrate, induced by duramycin, a tetracyclic antibiotic peptide with 19 amino residues. Ultrasonic homogenization generated a suspension mainly consisting of minimal lipid particles (MLP) from 1-palmitoyl-2-oleoyl-*sn*-glycero-3-phosphocholine (POPC), and 1-palmitoyl-2-oleoyl-*sn*-glycero-3-phosphoethanolamine (POPE) in a phosphate buffer solution, confirmed by dynamic light scattering (DLS). *In situ* STM discerned individual MLP as particles (diameter ~8 nm) spread on Au(111), modified with alkanethiol, within the suspension. The MLP became fragile by the presence of duramycin, and the MLP were easily scratched by the scanning tip into multilayers along the surface. This process of particle fusion on the gold surface coincides with the aggregation of MLP in the suspension, observed by DLS. It was demonstrated that STM is capable of discerning and monitoring the nanometer-scale features of phospholipid particles altered by antibiotics with biochemical impact. STM might allow *in situ*, real-space, nanometer-scale observations of minute particles composed of phospholipids within the real cells with the highest magnification ratio.

## Introduction

Thousands kinds of phospholipids are found in the natural cell membrane, assembled into nanometer-scale microstructures to realize physiological functions.<sup>1–4</sup> Microstructures of phospholipids, such as transport vesicles,<sup>5</sup> play an important role in protein recognition and material transportation in single molecular scale. Such lipid-wrapped particles recognized as organelles in real cells are of the sizes larger than 100 nm. Lipid particles of 10 nm scale, which have not been recognized because of lack of detecting methods, may exist in the real cells and may play important roles, such as they may carry materials and information across the cells. It is usually difficult to detect such small intact objects *in vivo* or *in vitro*. Scanning tunneling microscopy (STM), which was originally invented to magnify inorganic solid surfaces,<sup>6</sup> is nowadays applicable to soft materials immersed in aqueous media.<sup>7,8</sup> The ultimately high magnifying capability of STM will bring about a new possibility in studies of morphological aspects in nanoscopic cell physiology.

We optimized our STM system for operation toward solid surfaces immersed in liquid. This allowed us to obtain the dynamic images of molecular layers before and after adding substances into the liquid that induce biochemical reactions at surfaces. This sort of STM operation, namely, *in situ* STM, is

compatible with electrochemical operation in aqueous solutions.<sup>9</sup> We could successfully observe a model cell membrane composed of phosphatidylcholine with two 6-carboned alkyl chains, which is soluble in water. We observed a series of structural changeover in the arrangement of lipid molecules driven by a control of the electrode potential.<sup>10</sup>

Antibiotic proteins and peptides work as protective and sometimes aggressive systems against bacterial infection. The effects are complementarily with the highly specific cell-mediated immune response.<sup>11</sup> The antibiotic activities of peptides are mostly expressed through physical cell membrane disruption, driven by phospholipid–peptide interaction.<sup>11–14</sup> To clarify the effects of antibiotic peptides, nanometer-scale microscopic methods are useful in direct observation of the dynamic morphology.

In this report, we describe our application of *in situ* STM to obtain information on the physical behavior of phospholipids and duramycin, an antibiotic peptide. We constructed a model particle system, composed of 1-palmitoyl-2-oleoyl-*sn*-glycero-3-phosphocholine (POPC) and 1-palmitoyl-2-oleoyl-*sn*-glycero-3-phosphoethanolamine (POPE), which are commonly found in real cell membranes. We also applied dynamic light scattering (DLS) to obtain the diameter distribution of phospholipid particles. Initially, we attempted to make the phospholipid aggregates as small as possible in aqueous buffer solutions so as to distribute the phospholipid molecules homogeneously along the substrate surface. As a result, we produced phospholipid particles with a diameter less than 10 nm, which are probably the smallest forms of phospholipid clusters in existence.

\*Corresponding author. E-mail: maki@riken.jp.

- (1) Rothman, J. E.; Lenard, J. *Science* **1977**, *195*, 743–753.
- (2) Hannun, Y. A. *J. Biol. Chem.* **1994**, *269*, 3125–3128.
- (3) Devaux, P. F. *Biochemistry* **1991**, *30*, 1163–1173.
- (4) Cerbon, J.; Calderon, V. *Biochim. Biophys. Acta* **1991**, *1067*, 139–144.
- (5) Rothman, J. E. *Nature* **1994**, *372*, 55–63.
- (6) Binning, G.; Rohrer, H.; Gerber, C.; Weibel, E. *Phys. Rev. Lett.* **1982**, *49*, 57–61.
- (7) Chi, Q. J.; Zhang, J. D.; Nielsen, J. U.; Friis, E. P.; Chorkendorff, I.; Canters, G. W.; Andersen, J. E. T.; Ulstrup, J. *J. Am. Chem. Soc.* **2000**, *122*, 4047–4055.
- (8) Sek, S.; Xu, S.; Chen, M.; Szymanski, G.; Lipkowski, J. *J. Am. Chem. Soc.* **2008**, *130*, 5736–5743.
- (9) Gao, X. P.; Hamelin, A.; Weaver, M. J. *Phys. Rev. Lett.* **1991**, *67*, 618–621.

- (10) Matsunaga, S.; Yokomori, R.; Ino, D.; Yamada, T.; Kawai, M.; Kobayashi, T. *Electrochem. Commun.* **2007**, *9*, 645–650.
- (11) Shai, Y. *Biopolymers* **2002**, *66*, 236–248.
- (12) Zasloff, M. *Nature* **2002**, *415*, 389–395.
- (13) Dathe, M.; Meyer, J.; Beyermann, M.; Maul, B.; Hoischen, C.; Bienert, M. *Biochim. Biophys. Acta* **2002**, *1558*, 171–186.
- (14) Shai, Y. *Biochim. Biophys. Acta* **1999**, *1462*, 55–70.

Duramycin (molecular weight = 2013) and its familial antibiotics (cinnamycin and so on) are tetracyclic peptides consisting of 19 amino residues and bind specifically to phosphatidylethanolamines (PE).<sup>15–22</sup> Because of this characteristic feature, duramycin has been used for studies to determine the distribution and metabolism of PE in cell membranes.<sup>23–25</sup> At the same time, studies to reveal the mechanism of duramycin binding with PE have been performed.<sup>26–29</sup> Iwamoto et al.<sup>22</sup> reported that the curvature of lipid layers play an important role in duramycin binding. Therefore, it is interesting to monitor, using *in situ* microscopic methods, the real-space nanometer-scale morphological changes of phospholipids under the influence of duramycin.

This report provides eight sets of experimental results, categorized by (1) whether the sample was pure POPC or POPC + POPE mixture, (2) whether the observation was made by STM on solid substrate or by DLS in liquid phase, and (3) whether duramycin was absent or present in the system. The Results and Discussion section systematically describes these results. We detected nanoparticles with a diameter of 8 nm as the major part both of pure POPC and POPC + POPE mixtures on surfaces. Using two independent techniques (STM and DLS, which are nicely complementary: one in real-space and the other in momentum-space), we explicitly demonstrated the process of particle fusion by duramycin specifically for POPC + POPE mixture.

## Methods and Materials

### *In Situ* Scanning Tunneling Microscope (*in situ* STM).

All *in situ* STM images were obtained using Nanoscope E (Veeco instruments Inc.). We utilized Pt/Ir (80:20) tips (“Nanotip”, Veeco). The tip was coated with nail polish to minimize the Faraday current in the electrolyte. The measurement was performed in a Teflon-PFA (PerFluoroAlkoxyethylene) cell (volume of liquid content = 2 mL), assembled with a Pt plate (6 mm × 20 mm) as the counter electrode and a Pt wire as the reference electrode. A phosphate buffer (0.05 M, pH = 7.0 ± 0.1, prepared by neutralization of Na<sub>2</sub>HPO<sub>4</sub> and NaH<sub>2</sub>PO<sub>4</sub> aqueous solutions) was used as the supporting electrolyte. The sample potential was kept at 0 V versus the Pt reference electrode, and the tip potential was –0.4 V versus the Pt reference electrode. The open circuit potential of the phospholipid/1-C<sub>8</sub>H<sub>17</sub>SH/Au(111) electrode was in the vicinity of 0 V versus Pt fluctuating within ±0.05 V. We controlled the sample potential constantly at 0.0 V versus Pt reference electrode to operate the STM with an adequate stability and to avoid undesired electrochemical reactions.

(15) Pridham, T. G.; Shotwell, O. L.; Stodola, F. H.; Lindenfelser, L. A.; Benedict, R. G.; Jackson, R. W. *Phytopathology* **1956**, *46*, 575–581.

(16) Shotwell, O. L.; Stodola, F. H.; Michael, W. R.; Lindenfelser, L. A.; Dworschack, R. G.; Pridham, T. G. *J. Am. Chem. Soc.* **1958**, *80*, 3912–3915.

(17) Kessler, H.; Steuernagel, S.; Will, M.; Jung, G.; Kellner, R.; Gillessen, D.; Kamiyama, T. *Helv. Chim. Acta* **1988**, *71*, 1924–1929.

(18) Hayashi, F.; Nagashima, K.; Terui, Y.; Kawamura, Y.; Matsumoto, K.; Itazaki, H. *J. Antibiot.* **1990**, *43*, 1421–1430.

(19) Choung, S. Y.; Kobayashi, T.; Takemoto, K.; Ishitsuka, H.; Inoue, K. *Biochim. Biophys. Acta* **1988**, *940*, 180–187.

(20) Sheth, T. R.; Henderson, R. M.; Hladky, S. B.; Cuthbert, A. W. *Biochim. Biophys. Acta* **1992**, *1107*, 179–185.

(21) Navarro, J.; Chabot, J.; Sherrill, K.; Aneja, R.; Zahler, S. A.; Racker, E. *Biochemistry* **1985**, *24*, 4645–4650.

(22) Iwamoto, K.; Hayakawa, T.; Murate, M.; Makino, A.; Ito, K.; Fujisawa, T.; Kobayashi, T. *Biophys. J.* **2007**, *93*, 1608–1619.

(23) Emoto, K.; Kobayashi, T.; Yamaji, A.; Aizawa, H.; Yahara, I.; Inoue, K.; Umeda, M. *Proc. Natl. Acad. Sci. U.S.A.* **1996**, *93*, 12867–12872.

(24) Emoto, K.; Umeda, M. *J. Cell Biol.* **2000**, *149*, 1215–1224.

(25) Iwamoto, K.; Kobayashi, S.; Fukuda, R.; Umeda, M.; Kobayashi, T.; Ohta, A. *Genes Cells* **2004**, *9*, 891–903.

(26) Wakamatsu, K.; Choung, S. Y.; Kobayashi, T.; Inoue, K.; Higashijima, T.; Miyazawa, T. *Biochemistry* **1990**, *29*, 113–118.

(27) Hosoda, K.; Ohya, M.; Kohno, T.; Maeda, T.; Endo, S.; Wakamatsu, K. *J. Biochem.* **1996**, *119*, 226–230.

(28) Machaidze, G.; Seelig, J. *Biochemistry* **2003**, *42*, 12570–12576.

(29) Machaidze, G.; Ziegler, A.; Seelig, J. *Biochemistry* **2002**, *41*, 1965–1971.

**Dynamic Light Scattering (DLS).** Dynamic light scattering (DLS) was applied to estimate the size of lipid aggregates suspended in aqueous solutions. DLS measurements were carried out using a compact goniometer (DLS/SLS-5000, ALV, Germany) coupled with a photon correlator. A 22 mW He–Ne laser (Uniphase, USA) was used as the light source, where the wavelength  $\lambda$  was 632.8 nm. The measurement was performed in a toluene bath maintained at 25 °C.

Time-correlation functions, which were data obtained from DLS measurements, were converted to characteristic decay time distribution functions  $G(\Gamma^{-1})$  as a function of a characteristic decay time  $\Gamma^{-1}$ , by the aid of the widely used CONTIN algorithm.<sup>36,37</sup> We can obtain the characteristic decay time and calculate the hydrodynamic diameter of particles via the Stokes–Einstein equation

$$D_h = \frac{k_B T}{3\pi\eta_0 D} \quad (1)$$

where  $D_h$  is the hydrodynamic diameter,  $k_B$  is the Boltzmann constant,  $T$  is the measurement temperature,  $\eta_0$  is the viscosity of the solvent, and  $D$  is the diffusion constant. In this experiment,  $\eta_0 = 0.89 \times 10^{-3}$  Pa·s (the value for pure water) and  $T = 25$  °C. When the decay of the correlation function is due to the displacement of particles by Brownian motion (diffusive mode), the diffusion constant  $D$  is calculated from the measured characteristic decay time with

$$\Gamma = Dq^2 \quad (2)$$

Also,  $\Gamma$  is the characteristic decay rate and  $q$  is the amplitude of the scattering vector, defined by

$$q = \frac{4\pi n}{\lambda} \sin\left(\frac{\theta}{2}\right) \quad (3)$$

Here,  $n$  is the refractive index of the scattering medium, and  $\theta$  is the scattering angle. In this experiment,  $n = 1.332$  (the value for pure water), and several values of  $\theta$  were chosen between 30° and 150°.

**Materials.** 1-Palmitoyl-2-oleoyl-*sn*-glycero-3-phosphocholine (POPC, purity >99%) and 1-palmitoyl-2-oleoyl-*sn*-glycero-3-phosphoethanolamine (POPE >99%) were the products of CHCl<sub>3</sub> solutions from Avanti Polar Lipids Inc. CHCl<sub>3</sub> (>99%), C<sub>2</sub>H<sub>5</sub>OH (spectroscopic grade), Na<sub>2</sub>HPO<sub>4</sub>·12H<sub>2</sub>O (>99%), NaH<sub>2</sub>PO<sub>4</sub>·2H<sub>2</sub>O (>98%), NaOH (ultrapure grade), and 1-C<sub>8</sub>H<sub>17</sub>SH (>97%) were obtained from Kanto Chemicals, Japan. The gold crystal was prepared from an Au wire (diameter 1 mm, purity >99.999%, Furuya Metals, Japan). The electrodes and wirings for the STM electrochemical cell were made from Pt (wires of 1 mm and 0.25 mm in diameter, and a sheet of 0.1 mm in thickness, purity >99.98%, Nilaco, Japan). Duramycin was stored as a solution in pure water (0.69 mM, purity 90–95%, Sigma-Aldrich).

**Preparation of the Au (111) Substrate.** As an atomically flat surface, we utilized a small (111) facet on a single-crystal gold bead, prepared by melting one end of a gold wire in a hydrogen–oxygen flame. This gold surface was covered with a 1-C<sub>8</sub>H<sub>17</sub>SH self-assembled monolayer by immersing into an 1 mM C<sub>2</sub>H<sub>5</sub>OH solution for 15 min, followed by rinsing in pure C<sub>2</sub>H<sub>5</sub>OH.<sup>30–32</sup> This hydrophobic surface was fixed on the *in situ* STM measurement cell. The desired solutions were poured into the cell for successive STM observation.

**Preparation of the Lipid-Containing Liquids.** According to our experience,<sup>10</sup> the optimum concentration of phospholipids to

(30) Twardowski, M.; Nuzzo, R. G. *Langmuir* **2003**, *19*, 9781–9791.

(31) Twardowski, M.; Nuzzo, R. G. *Langmuir* **2004**, *20*, 175–180.

(32) Doyle, A. W.; Fick, J.; Himmelhaus, M.; Eck, W.; Graziani, I.; Prudovsky, I.; Grunze, M.; Maciag, T.; Neivandt, D. J. *Langmuir* **2004**, *20*, 8961–8965.

form layers visible by STM is 0.2–0.3 mM. Meanwhile, the critical micelle concentration of POPC and POPE is very low, and it is anticipated to form liposomes at such concentrations. We attempted to make the lipid particles as small as possible by ultrasonic homogenization. By vortex mixing, formation of multilamella vesicles (MLV, diameter > 100 nm) is usually expected.<sup>33</sup> By sonication, small unilamella vesicles (SUV, diameter ~30 nm) produced from the MLV are reported.<sup>34,35</sup>

In the present observations, all phospholipids were stored in CHCl<sub>3</sub> at -30 °C. A portion of the CHCl<sub>3</sub> solution was extracted into a small glass vial of the desired volume, while CHCl<sub>3</sub> was allowed to evaporate in a N<sub>2</sub> gas. After evaporation, the 4.5 mL of phosphate buffer was added into this vial, vortexed and sonicated with an ultrasonic bath (US102, SND, Japan) for 10 min, followed by the homogenization by an ultrasonic homogenizer (UH-50; SMT, Japan) for 30 min. The size distribution of phospholipid aggregations produced by sonication was monitored by DLS. As the homogenization time was increased, the average particle size decreased and reached a sharp distribution around a minimum particle diameter. The size distribution is described in detail later. It took 30 min to achieve the minimum particle size for 4.5 mL of suspension. It took a longer period to obtain the minimum particle size for a larger volume of suspension. The final particle size distribution apparently did not depend on the initially mixed concentration of phospholipid below 2 mM. The suspensions for STM and DLS observation were adjusted to the desired concentration by diluting the homogenized suspension with the phosphate buffer.

## Results and Discussion

**In Situ STM: Pure POPC and POPC + POPE Mixtures.** The *in situ* STM observation of phospholipids was performed by pouring the phospholipid suspensions into the STM liquid cell, assembled with a 1-octanethiol-modified Au (111) substrate, immersed in the phosphate buffer. Just after 2–3 h, we could not observe any changes from 1-octanethiol-modified substrate. In addition, continuous STM scanning disturbed the adsorption of phospholipids onto the substrate. Therefore, we started to scan the images 24 h after the addition of phospholipids. *In situ* STM images for pure POPC and POPC + POPE are shown in Figure 1. The concentrations of lipid suspensions were 200 μM POPC and 200 μM POPC + 100 μM POPE, respectively. In both images, one can find particles sitting on the surface. To obtain STM images of individual particles, the range of total phospholipid concentration in the suspension was narrowly limited. At total concentrations lower than 100 μM, only surfaces of 1-octanethiol-modified Au (111) with characteristic vacancy islands were observed within one day. When the total concentration was higher than 400 μM, the particles seemed to pile up and the surface became invisible to STM due to the high resistivity of the thick layer.

The height values in Figure 1 and hereafter are indicated as the physical tip height differences between two levels. Usually, these values do not represent true heights of objects at the surface without the existence of the STM tip. In STM observation, the tip height difference is commonly smaller than the real height of biomolecules expected from its intact dimensions.<sup>7</sup> Biomolecules with sizes larger than a few nanometers are considered to have a high electric resistance, and the tip should be closer to the surface to maintain the tunneling current for imaging over

the molecules. In our previous STM observation of phospholipid layer,<sup>10</sup> observed heights by STM were much lower than the sizes of intact molecules. It is imaginable that the scanning process might involve penetration of tip into the adlayer, deformation of molecules, or nonlinear change of the tunneling resistance.

For pure POPC, particles were found to scatter over flat terrace areas. The average size of particles in Figure 1A is  $8.0 \pm 1.2$  nm, and the average height is  $0.4 \pm 0.1$  nm. In the underlying flat areas, some holes with diameters of several nanometers are observed. Imaging the shape of the holes for an extended period of time, they deform and slide along the surface. This means that the fluidic phospholipid monolayer was formed on the hydrophobic substrate, and this sort of mobility is characteristic of the monolayer composed of phospholipid on the thiol self-assembled monolayer.<sup>10</sup> The average depth of these holes is measured to be  $0.15 \pm 0.02$  nm in this image. This height is much smaller than the length of POPC molecules. However, in our previous report,<sup>10</sup> a lipid monolayer exhibited a similar height, and therefore, in the present case, we recognize this height corresponding to the monolayer.

In the image of POPC + POPE mixture, densely packed particles were observed. The average size of particles in Figure 1B is  $7.8 \pm 1.6$  nm, and the average height is 2.0 nm. This in-plane diameter is the smallest one found in our experiment, and hereafter, we denote these smallest POPC + POPE aggregations as “minimal lipid particles” (MLP).

These STM observations of phospholipid particles are surprising to us, in terms of the low electric conductivity anticipated from the size of molecules and particles. Our results clearly show the fact that we can apply *in situ* STM to phospholipid layer and MLP, and we could recognize the MLP with an adequate spatial resolution of nanometers. This means that the electrons can tunnel thorough the phospholipid layers fast enough for STM imaging.

In order to examine that the phospholipid molecules are not fragmented by the ultrasonic agitation with large power, we tested the sonicated pure POPC and POPC + POPE MLP suspensions by thin layer chromatography with CHCl<sub>3</sub> + CH<sub>3</sub>OH + H<sub>2</sub>O + CH<sub>3</sub>COOH (65:43:3:1)<sup>38</sup> as the extension solvent. Only POPC and POPE were detected and no sign of fragmented phospholipids, such as single-stranded ones, were detected. MLP was confirmed to be composed of purely POPC or POPC + POPE.

As anticipated from the sharp size distribution of the MLP observed in the STM measurements (i.e.,  $8.0 \pm 1.2$  nm or  $7.8 \pm 1.6$  nm), MLP must be a nearly uniquely structured organization of phospholipid molecules. To consider the geometrical model structure of MLP, the elementary dimensions of the component molecules should be assumed. The dimensions of POPC and POPE were estimated as 2 nm in length and  $0.68 \text{ nm}^2$  in cross section, with a cylindrical shape.<sup>39,40</sup> The thickness of the elementary bilayer was estimated to be ~4–5 nm by atomic force microscopic metrology.<sup>41,42</sup> It is difficult to assemble a complete bilayer-skinned liposome with a diameter of 8 nm from elementary blocks of such a size. Micelles, composed of a phospholipid monolayer, are also hardly imagined as the model structure of MLP, because the attractive force for the hydrophobic part of the

(33) Nayar, R.; Hope, M. J.; Cullis, P. R. *Biochim. Biophys. Acta* **1989**, *986*, 200–206.

(34) Maulucci, G.; De Spirito, M.; Arcovito, G.; Boffi, F.; Castellano, A. C.; Briganti, G. *Biophys. J.* **2005**, *88*, 3545–3550.

(35) Huang, C. H. *Biochemistry* **1969**, *8*, 344.

(36) Provencher, S. W. *Comput. Phys. Commun.* **1982**, *27*, 213–227.

(37) Chu, B. *Laser light scattering*; Academic Press: London, 1991.

(38) Owens, K. *Biochem. J.* **1966**, *100*, 354–&.

(39) Kucerka, N.; Tristram-Nagle, S.; Nagle, J. F. *J. Membr. Biol.* **2006**, *208*, 193–202.

(40) Leekumjorn, S.; Sum, A. K. *Biophys. J.* **2006**, *90*, 3951–3965.

(41) Muresan, A. S.; Lee, K. Y. *C. J. Phys. Chem. B* **2001**, *105*, 852–855.

(42) Kim, Y. H.; Rahman, M. M.; Zhang, Z. L.; Misawa, N.; Tero, R.; Urisu, T. *Chem. Phys. Lett.* **2006**, *420*, 569–573.

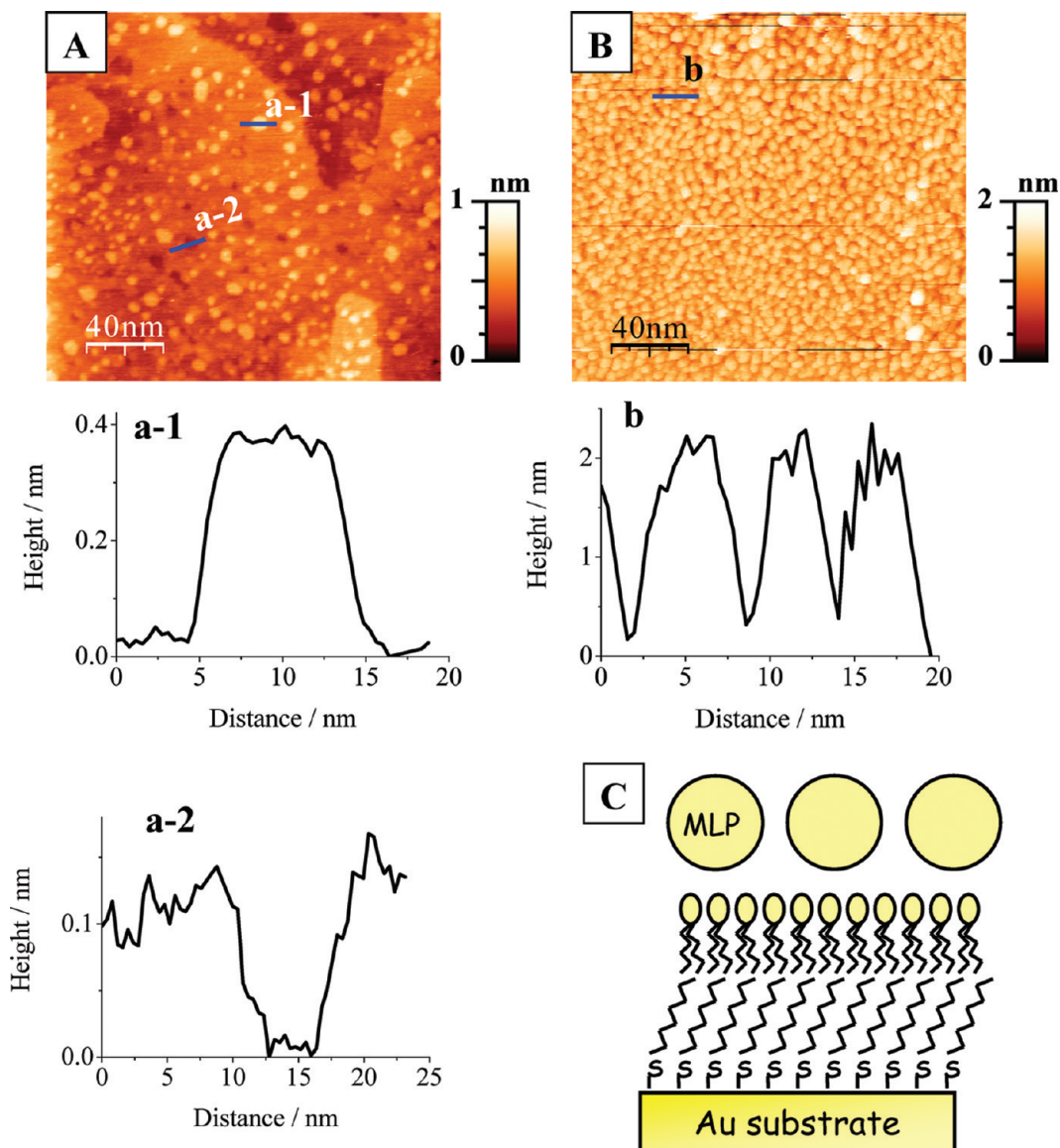


**Figure 1.** *In situ* STM images of phospholipids on a 1-C<sub>8</sub>H<sub>17</sub>S self-assembled monolayer on Au(111) in the phosphate buffer. Here, the STM bias voltage = -0.4 V, and the preset tunneling current = 1.5 nA. (A) with a pure POPC suspension adjusted at 200 μM in the cell. (B) with 200 μM POPC + 100 μM POPE suspension. Both images were obtained after 24 h from setting the substrate in the suspension of phospholipids. Plots of a-1, a-2, and b are the line profiles along the lines shown in each images. (C) A schematic cross-sectional view of the minimal lipid particles (MLP) are located over a monolayer of phospholipids, covering the hydrophobic 1-C<sub>8</sub>H<sub>17</sub>S self-assembled monolayer on Au (111).

phospholipid is not guaranteed for the integration of a particle. Okahata et al.<sup>43</sup> reported that amphiphilic molecules which have a similar structure to phospholipids can form a disk-like aggregate. Lyubartsev<sup>44</sup> predicted, by molecular dynamics simulations, disk-shaped phospholipid particles with a diameter of approximately 10 nm. This sort of disk-shaped particles agrees fairly well with the diameter of MLP in terms of diameter.

We consider MLP as the smallest stable or metastable form of phospholipid aggregations in aqueous media, as MLP were generated at the end of a rigorous homogenization procedure. No smaller particles were found after longer homogenization periods, with different concentrations or compositions of phospholipids, at room temperature. As a small stable aggregation of phospholipid, SUV (30 nm or larger in diameter) has been well recognized.<sup>34,35</sup>

We have no information about the relative thermodynamic stability of MLP compared with SUV and larger phospholipid objects. Anyway, within the longest period of our observation, MLP did not change in size and were practically stable.

The structure of composite layers observed by *in situ* STM, shown in Figure 1A,B, can be elucidated by the hydrophobicity of the components. It is obvious that the outer sphere of MLP is all filled with the hydrophilic parts. On the other hand, the substrate surface covered with a 1-C<sub>8</sub>H<sub>17</sub>S self-assembled monolayer is firmly hydrophobic. When such a hydrophobic surface is in contact with a phospholipid suspension, a monolayer of phospholipid will be immediately formed, delivered from an undetectably small amount of freely dissolved molecules or by particle fusion at the surface. The depths of the holes in Figure 1A, 0.15 nm, are similar to the lipid monolayer height in our previous work,<sup>14</sup> and this supports the existence of a phospholipid monolayer over the 1-octanethiol self-assembled monolayer. Then, the surface covered with the phospholipid monolayer becomes hydrophilic, and we can

(43) Okahata, Y.; Ihara, H.; Shimomura, M.; Tawaki, S.; Kunitake, T. *Chem. Lett.* **1980**, 1169–1172.

(44) Lyubartsev, A. P. *Eur. Biophys. J. Biophys. Lett.* **2005**, *35*, 53–61.

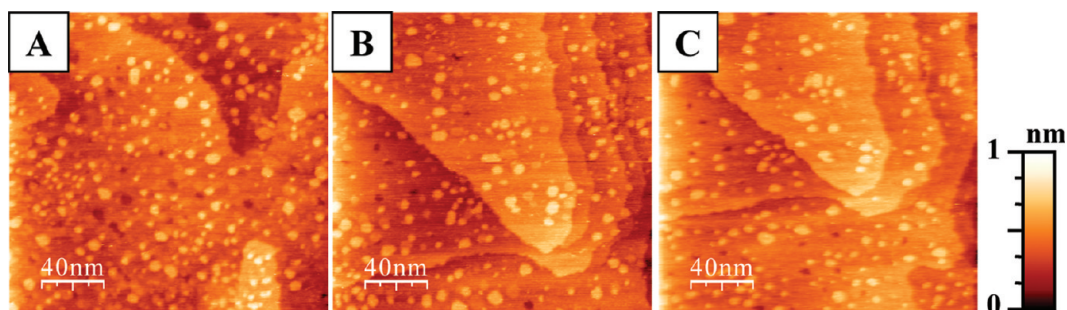


**Figure 2.** *In situ* STM images of phospholipids on a 1-C<sub>8</sub>H<sub>17</sub>S self-assembled monolayer on Au(111) in the phosphate buffer. Here, the STM bias voltage = -0.4 V, and the preset tunneling current = 1.5 nA. (A) With pure POPC suspension adjusted at 200 μM in the cell. (B) Right after the addition of 7 μM duramycin to A. (C) After 10 minutes of continuous STM scans following B.

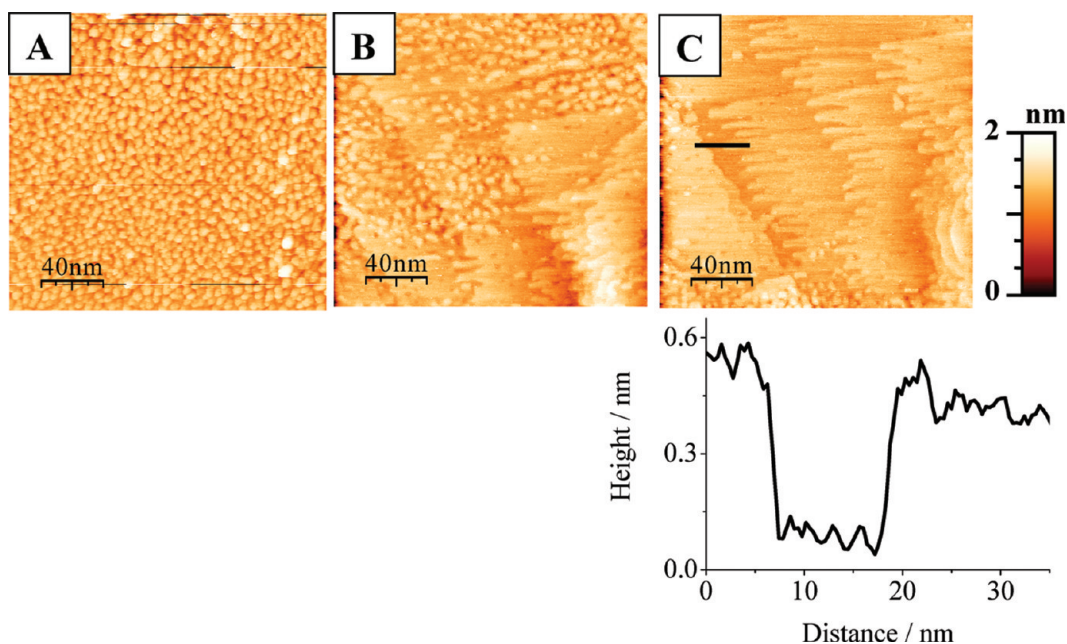


**Figure 3.** *In situ* STM images of phospholipids on a 1-C<sub>8</sub>H<sub>17</sub>S self-assembled monolayer on Au(111) in the phosphate buffer. Here, the STM bias voltage = -0.4 V, and the preset tunneling current = 1.5 nA. (A) With 200 μM POPC + 100 μM POPE suspension in the cell. (B) Right after the addition of 7 μM duramycin to A. (C) 10 minutes of continuous STM scans following B. The line profile along the black horizontal segment in C is shown in the plot below.

conclude the model structure shown in Figure 1C. The MLP are attracted to the surface by a certain strength of the attractive interaction between hydrophilic parts in phospholipids.

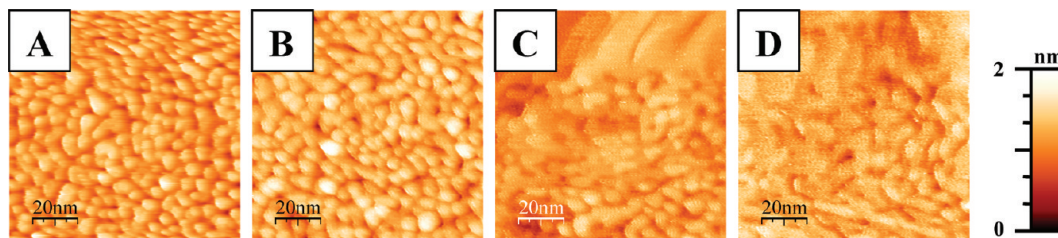
***In Situ* STM: With duramycin, Pure POPC and POPC + POPE Mixtures.** Duramycin dissolved in pure water (0.69 mM) was added to the *in situ* STM cell containing the Au substrate precovered with MLP of pure POPC or POPC + POPE. The concentration of duramycin in the cell was adjusted to be 7 μM. Pure POPE did not form a stable layer on the substrate, and we could not always obtain STM images.

Figure 2 shows a series of *in situ* STM images of pure POPC MLP after the addition of duramycin. *In situ* STM images were obtained before the addition of duramycin (A), immediately after the addition (B), and 10 min later with several frames of STM scanning (C). Except for frame relocation, due to a mechanical drift, the common sizes and shapes of particles exhibit no significant change. By comparing Figure 2B and C, almost exactly the same particles stay in the same places. Duramycin caused no significant change in the images of pure POPC layer.

Note that duramycin induced a drastic change on the POPC + POPE MLP. Figure 3 shows the sequence before (A) and after (B,C) the addition of duramycin. Before the addition, the MLP layer was stable and images similar to Figure 3A were

constantly obtained. Immediately after the injection of duramycin (Figure 3B), the particle features were lost, as seen in the lower half of the frame. The area was occupied with a few terraces with elongated wavy edges shaped like the teeth of a comb. The width of each tooth matches in size the diameter of the MLP. The direction of the elongation is parallel to the rapid scanning lines of STM. This change indicates that the existence of duramycin immediately destabilized the MLP to be vulnerable to the STM tip. Figure 3C was recorded after some tens of scans over the same area. Most of the MLP lost their particle shape, and terraces (with comb-shaped edges dragged along the scanning direction) were observed. These images visually demonstrate the particle fusing effect of duramycin to POPC + POPE MLP, which became fragile and were easily broken when the STM tip touched them. Duramycin molecules were obviously involved within these frames; however, we could not discern individual molecules of duramycin. According to nuclear magnetic resonance analysis, the diameter of duramycin single molecules is estimated to be less than 2 nm.<sup>45</sup> It is difficult to point out features of this size over the crowd of objects composed of lipid.

(45) Zimmermann, N.; Freund, S.; Fredenhagen, A.; Jung, G. *Eur. J. Biochem.* **1993**, *216*, 419–428.



**Figure 4.** *In situ* STM images of phospholipids on a 1-C<sub>8</sub>H<sub>17</sub>S self-assembled monolayer on Au(111) in the phosphate buffer. Here, the STM bias voltage = -0.4 V, and the preset tunneling current = 1.0 nA. (A) With 200  $\mu$ M POPC + 50  $\mu$ M POPE suspension in the cell. The distortion of the upper part was due to an occasional thermal drift. (B) 20 minutes after the addition of 7  $\mu$ M duramycin to A. (C) Right after the addition of 14  $\mu$ M duramycin to A. (D) 10 minutes of continuous STM scans following C.

A similar series of *in situ* STM images depicting the POPC + POPE MLP fusion process is shown in Figure 4. The MLP were prepared at concentrations of 200  $\mu$ M POPC + 50  $\mu$ M POPE. Before the addition of duramycin (Figure 4A), the particle size distribution in that image was  $7.9 \pm 0.9$  nm, about the same as that for 200  $\mu$ M POPC + 100  $\mu$ M POPE (Figure 3A). When 7  $\mu$ M of duramycin was added, no significant change was observed in 20 min (Figure 4B). Then, after more duramycin was added, reaching a total concentration of 14  $\mu$ M, the fusion process started immediately (Figure 4C). Again, a step-terrace structure composed of phospholipid was left over. As the concentration of POPE was lower than in the case of Figure 3, more duramycin was needed to start fusing MLP.

The effect of duramycin specifically to MLP containing POPE was confirmed. We can estimate the number of phospholipid molecules by considering the dimensions of POPC and POPE (2 nm in length, and  $0.68 \text{ nm}^2$  in cylindrical cross section).<sup>39,40</sup> If we assume MLP to be disk-shaped aggregations, approximately 200 molecules of this size compose MLP with a diameter of 8 nm; the same can be said for the mixtures 200  $\mu$ M POPC + 100  $\mu$ M POPE (Figure 3) and 200  $\mu$ M POPC + 50  $\mu$ M POPE (Figure 4).

Then, the number of POPE molecules on the MLP surface is estimated to be approximately 67 or 40, respectively, if we assume that the initial mixing ratio of POPC + POPE in suspension is maintained on the MLP surface. As the number of POPE molecules on MLP decreases, more duramycin is necessary for MLP fusion. When the concentration of POPE on the MLP surface was low, a longer period of time was needed for the duramycin molecule to find a POPE to bind. It is interesting to note that the particle fusing activity of duramycin was expressed at such small amounts.

The flat layer formed after the MLP fusion is interpreted to be composed of bilayers of phospholipids. In general, a bilayer is a stable form of phospholipid in water. In Figure 3C or Figure 4D, the outermost surface is in contact with water and the hydrophilic parts of phospholipids should be facing the outer surface. The step heights measured at the edge of the terraces in Figure 3C and Figure 4D were  $0.5 \pm 0.1$  nm, and the heights of all steps in the frame were about the same. Although the step height of 0.5 nm is again smaller than the expected thickness of lipid bilayer, it is apparently larger than the monolayer height observed in Figure 1. From the viewpoint of STM observation, the ground level of the outer surface should be parallel to the substrate surface plane. The most rational interpretation we consider is that one or more bilayers are laid parallel to each other and slightly lifted up, at a small angle from the substrate surface. At the observed step edges, another lipid layer goes underneath the neighboring layer.

**DLS: Pure POPC and POPC + POPE Mixtures.** Dynamic light scattering (DLS) was applied for POPC/POPE suspensions, to estimate the particle size as well as to confirm the effect of duramycin in the solution phase. We prepared a pure

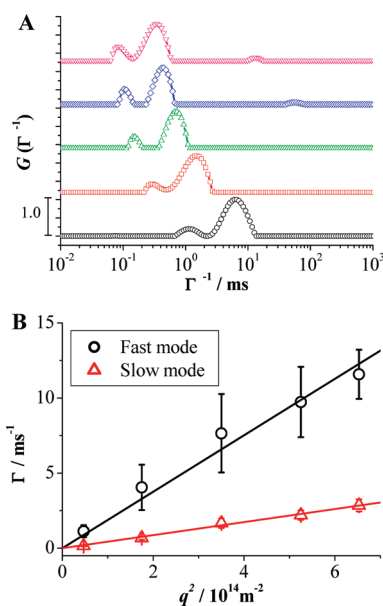


**Figure 5.** (A) Dynamic light scattering (DLS) data for a 200  $\mu$ M POPC suspension in the phosphate buffer, after ultrasonic homogenization for various scattering angles. The incident light wavelength was 632.8 nm, and the liquid temperature was 25°C. Scattering angles were  $\theta = 30^\circ$  (○),  $60^\circ$  (□),  $90^\circ$  (Δ),  $120^\circ$  (◇),  $150^\circ$  (▽). (B)  $q^2$  versus  $\Gamma$  plots made separately for the “fast mode” (○) and the “slow mode” (Δ) from A. The peak values of  $\Gamma$  are plotted as functions of  $q^2$ , calculated using eq 3. The slopes of these two lines are converted into the hydrodynamic diameters of the particles, which are 26.0 nm for the fast mode and 112.6 nm for the slow mode, by means of the Stokes–Einstein equation (eq 1).

POPC suspension (200  $\mu$ M), and a POPC + POPE (POPC: POPE = 200  $\mu$ M: 100  $\mu$ M) mixed suspension in a 0.05 M phosphate buffer. These concentrations were the same as that for *in situ* STM observation. For the pure POPE system, an oily phase was formed and separated from the buffer solution, and thus it was unable to prepare a homogeneous sample for DLS.

The DLS result for a pure POPC system is shown in Figure 5 as  $\Gamma^{-1}$  versus  $G(\Gamma^{-1})$  plots, where  $G$  is the intensity distribution function normalized by the maximum value on each curve. For all values of  $\theta$  studies, two peaks were found to shift along the  $\Gamma^{-1}$  axis, where the two peaks, at small and large  $\Gamma^{-1}$ , correspond to a “fast mode” and a “slow mode”, respectively. The plots in Figure 5B show the relationship between  $q^2$  and  $\Gamma$ . Both in the fast and slow modes,  $\Gamma$  is proportional to  $q^2$ , consistent with eq 2, indicating that the scattering dynamics is in the diffusive mode. Two types of particles with different average hydrodynamic diameters coexisted in the suspension. In Figure 6, the DLS for pure POPC system and POPC + POPE system are compared at  $90^\circ$  of the scattering angle. Also in the POPC + POPE mixture, two kinds of particles were formed in the solution.

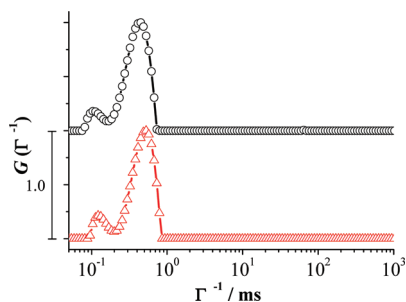


**Figure 6.** The DLS  $\Gamma^{-1}$  versus  $G$  data for ultrasonically homogenized suspensions of 200  $\mu\text{M}$  pure POPC ( $\circ$ ) and 100  $\mu\text{M}$ : 200  $\mu\text{M}$  POPC + POPE mixture ( $\Delta$ ), obtained for a  $90^\circ$  scattering angle, at  $25^\circ\text{C}$ .

The hydrodynamic diameters of these particles, calculated from eqs 1 and 2, were 26.0 nm (fast mode) and 112.6 nm (slow mode), for both the pure POPC and also the POPC + POPE mixtures. It was also found that this MLP suspension was stable. The size distribution and the shape of these particles did not change after one day. The standard deviations for these two diameters are small compared to generic particle suspensions, and in our case, the two different diameters were clearly resolved.

From the ratio of these peak heights of distribution functions, we can estimate the number ratio of these two components according to the bimodal distribution theory by Shibayama et al.<sup>46</sup> With this theory, the distribution function  $G_i(\Gamma^{-1})$  for the each particle size is given by

$$G_i(\Gamma^{-1}) \propto N_i R_i^6 \Phi^2 \quad (4)$$

where  $R_i$  and  $N_i$  are the radius and the number of each particle in the detection volume, respectively. The peak index is denoted by  $i$ , and  $\{\Phi(qR_i)\}^2$  is the form factor. This form factor is approximated as

$$\{\Phi(qR_i)\}^2 \cong \begin{cases} 1 & qR_i < 1.78 \\ 1.78^4 (qR_i)^{-4} & qR_i > 1.78 \end{cases} \quad (5)$$

The values  $R_1 = 13.0$  nm and  $R_2 = 56.3$  nm were obtained as explained above, and the values of  $qR$  correspond to 0.24 and 1.05, respectively. Thus,  $\{\Phi(qR_i)\}^2$  can be replaced by 1 and hence  $G_i(\Gamma^{-1}) \propto N_i R_i^6$ . The number ratio of these particles, calculated by curve fitting to Figures 4 and 5, becomes (112.6 nm particles): (26 nm particles) = 0.03:99.97, which is a ratio common for pure POPC and POPC + POPE mixtures. Most of the phospholipid molecules formed particles with a 26 nm diameter. Although the scattering intensity for the peak at 26 nm is smaller than that for 112.6 nm, the scattering efficiency for small particles overcompensates this, leading to such population numbers.

From the particle populations, the MLP with an average diameter of 8 nm, observed by STM, are considered here to be the same particles, observed by DLS, with a hydrodynamic diameter of 26 nm. In Figure 1B, approximately 1200 MLP are counted; all of these with essentially the same diameter. More than 99.9% of phospholipid particles were observed by STM to be MLP. However, in DLS, no peaks other than for 26 and 112.6 nm were recognized in the whole range of  $\Gamma^{-1}$ . The DLS distribution function indicated that the suspensions were nearly purely composed of particles with a hydrodynamic diameter of 26 nm. The dominant particles visualized in real space by STM should then be the dominant particles also detected in momentum space by DLS, despite a significant apparent mismatch in the estimated diameters. The resolution of this apparent

contradiction is that STM provides a direct diameter and DLS an effective hydrodynamic diameter.

In general, microscopic particle diameters are smaller than the hydrodynamic diameters derived by eq 1 from DLS diffusion constant.<sup>47</sup> For example, Au nanoparticles with a diameter of 9 nm were observed<sup>48</sup> by scanning electron microscopy. For the same nanoparticle suspension, DLS gave<sup>48</sup> an average diameter of 13 nm. It is anticipated that the hydrodynamic diameter provided by DLS involves solvent, solute and surfactant molecules dragged around the core particle, resulting in slow motion. The softness of the particle core, made of phospholipid, will also matter with hydrodynamic motion. When the particle diameter is on the order of 10 nm, the surrounding fluid cannot be always considered continuous, and the fluid viscosity deviates from the macroscopic value. Actually, a deviation of 200 times in the diffusion coefficient was observed<sup>49</sup> for CdSe nanoparticles. A molecular dynamics simulation<sup>50</sup> predicted an increased local viscosity of water around nanoparticles, taking into account the roughness of particle surfaces and the molecular-scale  $\text{H}_2\text{O}$ –particle interaction. In the present case, the hydrodynamic diameter is three times larger than the STM core diameter. This mismatch is among the deviations found or estimated in those recent studies on nanoparticles.

**DLS: With Duramycin, Pure POPC and POPC + POPE Mixtures.** We added duramycin to pure POPC and the POPC + POPE mixture suspensions and monitored their change using DLS. The distribution functions are shown in Figure 7, in which the observed scattering angle was  $90^\circ$ .

For a pure POPC MLP suspension, the addition of 7  $\mu\text{M}$  of duramycin gave no recognizable change in DLS, as shown in Figure 7A. In the case of POPC + POPE, the distribution function changed as duramycin was added step by step (Figure 7B). Upon mixing 7  $\mu\text{M}$  of duramycin, three peaks were observed. Two peaks are at the same positions as before the addition of duramycin, while a new large peak appeared in the higher  $\Gamma^{-1}$  region. The peak at the 6 ms characteristic decay time ( $\Gamma^{-1}$ ) in Figure 7B is converted into a hydrodynamic diameter of about 1000 nm. Some amount of MLP still remained in the suspension, and the rest was fused into larger particles. This aggregation observed by DLS corresponds to the MLP fusion observed by *in situ* STM, as shown in Figure 3. We can recognize the fusion of POPC + POPE MLP into one spread layer over the frame of a 200 nm  $\times$  200 nm square after duramycin was added. DLS indicated the formation of particles with diameters larger than 1000 nm. This size exceeds the size of the STM frame. We consider that MLP fusion into flat layers observed by STM is identical to the formation of large vesicles in suspension revealed by DLS. Upon further addition of duramycin, the peak of MLP completely disappeared. At higher concentration of duramycin, the measurement was sometimes disturbed by an enhanced turbidity in the solution. Even some white precipitates were visually observed, indicating an intensive aggregation of phospholipid and duramycin. A similar process of particle fusion was observed, as an increase in turbidity, by an antibiotic reaction with artificial amphiphilic molecules and haptens.<sup>51,52</sup>

(47) Burchard, W. In *Branched Polymers II*; 1999; Vol. 143, pp 113–194.

(48) *NIST Report of Investigation Reference Material 8011*; U.S. National Institute of Standards & Technology; Gaithersburg, MD; 2007.

(49) Tuteja, A.; Mackay, M. E.; Narayanan, S.; Asokan, S.; Wong, M. S. *Nano Lett.* **2007**, *7*, 1276–1281.

(50) Heyes, D. M.; Nuevo, M. J.; Morales, J. J. *J. Chem. Soc., Faraday Trans.* **1998**, *94*, 1625–1632.

(51) Ihara, H.; Arimura, T.; Imamura, T.; Satoh, E.; Kunitake, T.; Hirayama, C. *Polym. J.* **1992**, *24*, 1017–1024.

(52) Ihara, H.; Imamura, T.; Kunitake, T.; Hirayama, C. *Clin. Chim. Acta* **1988**, *175*, 51–58.

(46) Shibayama, M.; Karino, T.; Okabe, S. *Polymer* **2006**, *47*, 6446–6456.

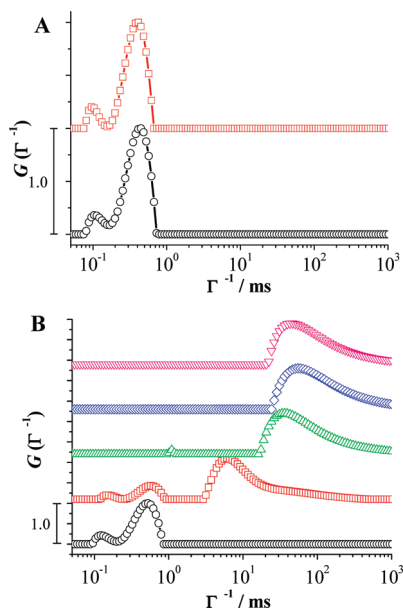


**Figure 7.** The DLS  $\Gamma^{-1}$  versus  $G$  data for ultrasonically homogenized suspensions of phospholipids in the phosphate buffer, obtained at  $90^\circ$  of the scattering angle. The liquid temperature is  $25^\circ\text{C}$ . (A) Suspension of pure  $200\ \mu\text{M}$  POPC before and after the addition of  $7\ \mu\text{M}$  duramycin in the cell. (B) Suspension of  $100\ \mu\text{M}/200\ \mu\text{M}$  POPC + POPE mixture, after the stepwise addition of duramycin. The duramycin concentration in the measurement cell was zero ( $\circ$ ),  $7\ \mu\text{M}$  ( $\square$ ),  $42\ \mu\text{M}$  ( $\Delta$ ),  $100\ \mu\text{M}$  ( $\diamond$ ), and  $150\ \mu\text{M}$  ( $\nabla$ ).

With an unprecedented level of magnification by *in situ* STM, we managed to visualize the nature of POPC and POPE molecules assembled into the MLP, and to discern the particle fusion caused by duramycin. This allowed us to observe many features at the nanometer scale. Independently, using DLS, we observed the aggregation of MLP by addition of duramycin. By combination of *in situ* STM and DLS, we also studied the same phenomenon in liquid phase. Therefore, we could study the physical behavior of phospholipid molecular assemblies both in real space and in momentum space.

Although MLP has not been explicitly recognized in real cells, MLP are considered an elementary form of phospholipids being transported in cells. Because of the smallest size as particles, MLP are of fundamental importance in considering the physical aspects of intracellular transportation in general. It has been suggested that phospholipid liposomes work as transportation media,<sup>53–56</sup> but the mechanisms are still unclear in detail. The transportation processes have been considered to involve proteins bound with phospholipid. Kobayashi et al.<sup>57</sup> reported that pure phospholipid vesicles were transported with a definite direction and the size of phospholipid aggregations was related with the rate of transportations. These preceding findings imply that there might be some invisible objects participating in the transportation phenomena in cells.

In this work, we recognized MLP standing at the physically smallest limit of objects composed of phospholipid. The signifi-

cant effect of antibiotic peptide to MLP is also interesting in considering the cell biological functions of MLP. Therefore, in cell physiological and biochemical senses, it will be helpful to imagine MLP as the smallest player in real cells in general. On the basis of such facilitation of nanometer-scale imaging, STM is a promising tool to analyze the physicochemical aspects of cell-membrane physiology and moreover to develop unprecedented analysis of nanometer-scale intracellular organelles.

## Conclusion

We applied both *in situ* STM and dynamic light scattering (DLS) to understand, at the nanometer scale, the effect of duramycin on phospholipid particles in aqueous media. Below, we provide a more detailed and itemized list of our results.

1. Aqueous phospholipid suspensions of pure POPC and POPC + POPE mixtures were prepared by rigorous ultrasonic homogenization and introduced over a  $1\text{-C}_8\text{H}_{17}\text{SH}$ -modified Au (111) substrate to perform *in situ* STM observations. Particles with a diameter of approximately 8 nm, designated as “minimal lipid particles (MLP)”, were found to form for both the pure POPC and the POPC + POPE mixture. By addition of a small amount of duramycin, only POPC + POPE MLP were observed to fuse with each other immediately, forming a continuous overlayer on the substrate.

2. Observation of the same suspensions by dynamic light scattering (DLS) indicated that almost all phospholipid molecules were contained in MLP. The addition of a small amount of duramycin induced the conversion of MLP into particles with diameters of about 1000 nm, only in POPC + POPE suspension. This process of particle fusion coincides with the formation of the continuous overlayer observed by STM on the solid substrate.

3. The highly leveraged effect of duramycin specifically worked only for MLP containing POPE. The selective membrane-fusing nature of duramycin has been visualized at the nanometer scale.

It was beyond our expectation that phospholipid particles with diameters of about 10 nm were visible to STM, since the electronic conductivity of such particles had been unknown. The *in situ* observation on aqueous solution is one notable advantage in STM observation, and this strong point was fully utilized to detect the effects of antibiotics on particles. We now recognize that *in situ* STM is basically applicable to the minute biological world of some tens of nanometers and can also acquire live movies. We hope that the present microscopic observations will contribute to understanding the physicochemical nature of antibiotic peptides interacting with cell membranes, and provide a promising approach toward the overall physiological elucidation and pharmaceutical development of antibiotics.

**Acknowledgment.** This work was supported in part by the RIKEN President Discretionary Fund (2004–2006). Grants-in-Aid for Scientific Research on Promotion of Novel Interdisciplinary Based on Nanotechnology and Materials and Global COE Program “the Physical Sciences Frontier”, MEXT, Japan. S. Matsunaga acknowledges the support from Research Fellowships for Young Scientists of the Japan Society for the Promotion of Science. We are thankful to Dr. Franco Nori for his critical reading of the manuscript preparation.

(53) Clague, M. J. *Biochem. J.* **1998**, *336*, 271–282.

(54) Lane, J.; Allan, V. *Biochim. Biophys. Acta* **1998**, *1376*, 27–55.

(55) Allan, R. B.; Balch, W. E. *Science* **1999**, *285*, 63–66.

(56) Urbani, L.; Simoni, R. D. *J. Biol. Chem.* **1990**, *265*, 1919–1923.

(57) Kobayashi, T.; Pagano, R. E. *Cell* **1988**, *55*, 797–805.